Journal of Solid State Chemistry **151,** 77–84 (2000)
doi:10.1006/jssc.2000.8625, available online at http://www.idealibrary.com on IDEAL®

A New Orthorhombic $Ba_8Co_7O_{21}$ Phase: Polymorphism in the $(Ba_3Co_2O_6)_\alpha(Ba_3Co_3O_9)_\beta$ System

K. Boulahya, M. Parras, and J. M. González-Calbet[1]

Dpto. Química Inorgánica, Facultad de Ciencias Químicas, Universidad Complutense, 28040-Madrid, Spain

and

A. Vegas

Instituto de Química-Física Rocasolano, CSIC, Serrano 119, E28006-Madrid, Spain

Received November 2, 1999; in revised form December 27, 1999; accepted January 10, 2000

The systematic search of new intermediate phases between 2H-$BaCoO_3$ and $Ca_3Co_2O_6$ structures has shown, for the first time, the existence of polymorphism in monodimensional phases of the homologous series $(A_3B_2O_6)_\alpha(A_3B_3O_9)_\beta$. A new $Ba_8Co_7O_{21}$ phase, different from the trigonal phase previously reported, has been synthesized. The new material is orthorhombic (SG *Fd2d*) with unit cell parameters $a_o = 1.14$, $b_o = 1.98$, and $c_o = 1.75$ nm. Both orthorhombic and trigonal phases are built up of isolated rows of polyhedra parallel to the *c*-axis formed by one trigonal prism and six ocathedra sharing faces, but with a different spatial arrengement between the chains. The orthorhombic structure can be derived from a hcp stacking of Ba_8O_{24} and $Ba_8Co_2O_{18}$ layers.

Key Words: **$Ba_8Co_7O_{21}$ polymorphs; 2H related perovskite; Ba_8O_{24} and $Ba_8Co_2O_{18}$ hexagonal stacking; electron diffraction; high resolution electron microscopy.**

INTRODUCTION

The ordered intergrowth between the 2H-$BaNiO_3$ (1) and Sr_4PtO_6 (2) structural types has led to a series of compounds with the general formula $(A_3B_2O_6)_\alpha(A_3B_3O_9)_\beta$ (3) whose structures are made up of isolated rows of *B* octahedra and *A*′ trigonal prisms (*A*′ equal to or different from *B*), running along the *c*-axis, the *A* cations occupying coordination sites between the chains. Alternatively, these structures can be derived from a hcp stacking of A_3O_9 and A_3BO_6 layers. The different stoichiometries that can arise from a mixed packed of these layers have been discussed by Darriet and Subramanian (4).

In recent years, several systems have been reported with these characteristics. In most of them, the coordination polyhedra are occupied by cations of different chemical nature (5, 6). This is the case, for instance, for Sr_4PtO_6, where Pt is in octahedral (O) coordination and Sr is in a trigonal prism (P) environment. Mixed oxides with only one cation occupying both polyhedra have only been described for Co (7, 8) and Ni (9, 10).

The systematic study of the *A*–Co–O system (*A* = Ba, Sr, Ca) (3, 11, 12) has shown that the distance between *A* cations is one of the main factors governing the structural type which can be stabilized. From 2H-$BaCoO_3$ (13), the introduction of prisms in the structure is accompanied by a progressive decreasing of the c_{2H} parameter. Therefore, keeping *B* = Co, to increase the P/O ratio it is necessary to reduce the ionic radius of the *A* cation. Thus, when Ba is partially substituted by Sr, the P/O ratio increases up to 1P/4O for the $Sr_6Co_5O_{15}$ (7) composition. This P/O ratio can be increased up to 1P/1O for the $Ca_3Co_2O_6$ phase (8).

To prepare these materials, besides the adequate selection of the *A* cation, an accurate control of both temperature and annealing time is required. For instance, all samples up to now reported in the Ba–Co–O system (3, 11, 12) have been isolated at temperatures between 900 and 940°C. For Ba:Co = 8:7, the trigonal $Ba_8Co_7O_{21}$ phase is stabilized at 920°C for 5 days. Its structure can be described as formed by isolated chains running parallel to the *c*-axis, constituted by six octahedra and one trigonal prism sharing faces, both occupied by Co atoms, and separated by columns of Ba atoms. This structure shows a modulation along the direction perpendicular to the Co prism planes. This is a general feature of all these materials and can be associated with the displacement of such Co atoms with respect to the center of the trigonal prisms. The unit cell is trigonal (SG *P*321) with parameters $a = 0.99$ and $c = 1.75$ nm.

By keeping the same cationic ratio (8:7), a different phase is obtained when the treatment conditions are changed. We report in this paper the structure of a new orthorhombic

[1] To whom correspondence should be addressed.

0022-4596/00 $35.00

$Ba_8Co_7O_{21}$ phase which constitutes the first example of polymorphism of these monodimensional phases.

EXPERIMENTAL

The orthorhombic $Ba_8Co_7O_{21}$ phase was prepared by heating in air stoichiometric amounts of $BaCO_3$ and Co_3O_4 at 875°C for 6 days. The average cationic composition was established by inductive coupling plasma. The local composition in every crystal was determined by energy dispersive spectroscopy (EDS) on a JEOL scanning electron microscope JSM-8600 equipped with an energy-dispersive system LINK AN10000. Results are consistent with the nominal compositions. The oxygen content was determined within $\pm 10^{-2}$ from the average oxidation state of cobalt analyzed by titration using Mohr's salt.

Powder X-ray diffraction was performed on a Philips X'Pert diffractometer using Cu$K\alpha$ radiation. Selected area electron diffraction (SAED) was carried out on a JEOL 2000FX electron microscope, fitted with a double tilting goniometer stage ($\pm 45°$). High-resolution electron microscopy (HREM) was carried out on a JEOL 4000EX electron microscope, fitted with a double tilting goniometer stage ($\pm 25°$), by working at 400 kV. Samples were ultrasonically dispersed in *n*-butanol and transferred to carbon-coated copper grids. Image simulations were calculated using the MacTempas package.

RESULTS AND DISCUSSION

Figure 1 shows the powder X ray diffraction patterns corresponding to orthorhombic $Ba_8Co_7O_{21}$ (o-phase) and trigonal $Ba_8Co_7O_{21}$ (t-phase). As can be observed, both patterns show similar characteristics. The most intense reflections can be assigned to a 2H cell, suggesting that both samples keep the … hh … stacking sequence corresponding to 2H-$BaCoO_3$. Besides, the *c* parameter of the hexagonal subcell is, in both samples, smaller than that shown by the 2H phase. Such a decreasing of the *c* parameter has been associated in rhombohedral phases with the presence of some Co in prismatic coordination (12, 13). According to that, the new (8:7) sample seems to exhibit structural characteristics similar to those of the trigonal phase, i.e., a hexagonal stacking sequence of layers with Co atoms occupying both octahedral and prismatic holes. The additional ordering suggested by the presence of low-intensity maxima and the true symmetry and structure of the new phase have been elucidated by SAED and HREM.

Figure 2 shows the most relevant SAED patterns corresponding to o-$Ba_8Co_7O_{21}$. The most intense reflexions along the $[1\bar{2}10]_{2H}$ zone axis correspond to $(10\bar{1}0)_{2H}$ and $(0001)_{2H}$ planes (Fig. 2a). A four-fold modulated superstructure is also seen along $[20\bar{2}1]^*_{2H}$ and equivalent directions. The $[11\bar{2}0]_{2H}$ reciprocal plane is identical to the previous one. However, the SAED pattern along $[\bar{2}110]_{2H}$ seems to be different (Fig. 2b). Once again, the most intense reflexions correspond to $(01\bar{1}0)_{2H}$ and $(0001)_{2H}$ planes but only a two-fold superstructure appears along $[01\bar{1}1]^*_{2H}$. This fact suggests the lost of hexagonal symmetry.

A similar situation is observed in the SAED patterns along $[1\bar{1}00]_{2H}$ (Fig. 2c) and $[01\bar{1}0]_{2H}$ (Fig. 2d). The first one shows as strongest reflections the $(11\bar{2}0)_{2H}$ and $(0002)_{2H}$, an eight-fold modulated superstructure being observed along $[44\bar{8}2]^*_{2H}$. Only $(\frac{1}{2}\,\frac{1}{3}\,l)$ satellite reflexions with $l = \frac{1}{4}, \frac{1}{2}, \frac{3}{4}, 1$ are

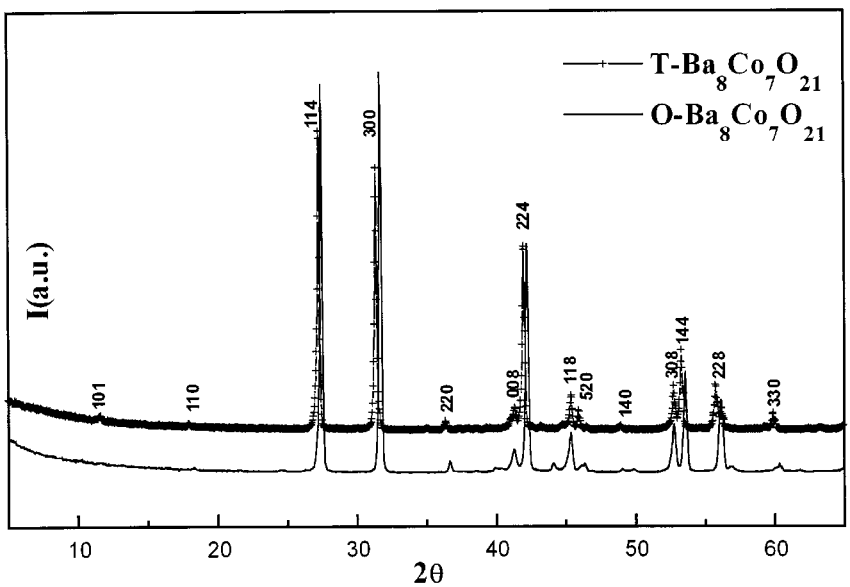

FIG. 1. Powder X-ray diffraction patterns corresponding to o-$Ba_8Co_7O_{21}$ and t-$Ba_8Co_7O_{21}$.

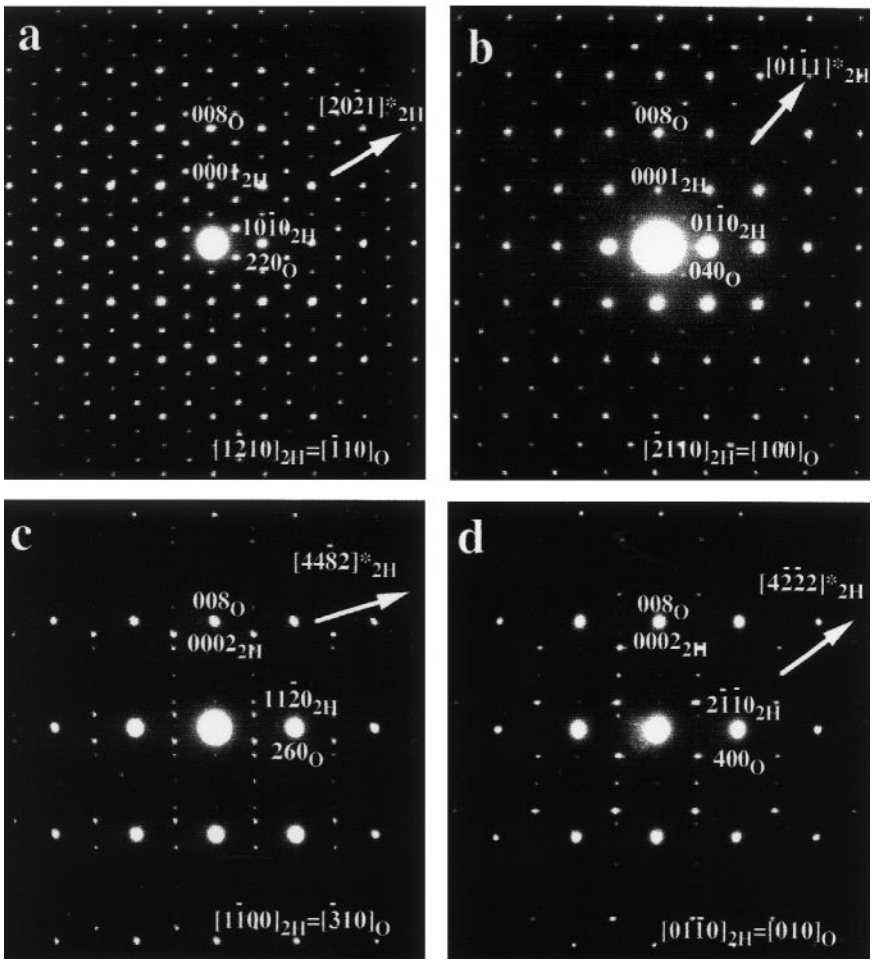

FIG. 2. SAED patterns corresponding to o-$Ba_8Co_7O_{21}$ along the following zone axes: (a) $[1\bar{2}10]_{2H}$, (b) $[\bar{2}110]_{2H}$, (c) $[1\bar{1}00]_{2H}$, and (d) $[01\bar{1}0]_{2H}$.

seen. The second one shows as strongest reflexions the $(2\bar{1}\bar{1}0)_{2H}$ and $(0002)_{2H}$, a four-fold superstructure being observed along $[4\bar{2}\bar{2}2]^*_{2H}$. Finally, the $[10\bar{1}0]_{2H}$ reciprocal plane is identical to that shown in Fig. 2c.

To confirm the true symmetry of this phase, a microdiffraction study has been carried out. Figure 3a shows the SAED pattern along $[0001]_{2H}$ and Fig. 3b the corresponding microdiffraction pattern. Only diffraction maxima corresponding to a hexagonal basic cell are observed in Fig. 3a. However, the microdiffraction pattern exhibits an *F..d* symmetry (14), confirming the orthorhombic symmetry.

On the basis of these results, all diffraction maxima can be indexed according to an orthorhombic unit cell (subindex o in previous figures) with parameters $a_o = 1.14$ nm $(2a_{2H})$, $b_o = 1.98$ nm $(2\sqrt{3}a_{2H})$, and $c_o = 1.75$ nm $(4c_{2H})$, with the following reflexion condictions:

$$00l,\ l = 4n;\ h00,\ h = 4n;\ 0k0\ k = 4n;$$

$$hk0,\ h + k = 4n,\ h,\ k = 2n.$$

$$0kl,\ k + l = 4n,\ k,\ l = 2n;\ h0l,\ h,\ l = 2n;$$

$$hkl,\ h + k,\ h + l,\ k + l = 2n.$$

Such systematic reflection conditions led to the *Fd2d* space group for the o-$Ba_8Co_7O_{21}$ phase. From these electron diffraction data, all X-ray diffraction maxima can be indexed as shown in Table 1.

To propose a structural model on the basis of these results, let us to emphasize that the most intense diffraction maxima correspond to the 2H subcell. This indicates that in the o-$Ba_8Co_7O_{21}$ phase, the hexagonal packing is maintained. Besides, the decreasing of the c_{2H} parameter corresponding to the orthorhombic phase $(c_o/4)$ can be associated with the presence of Co atoms in prismatic trigonal coordination. The formation of such prisms implies the substitution of BaO_3 layers by $BaCo_xO_{3-3x}$ layers $(0 \le x < 1)$.

On the other hand, the layer symmetry must be compatible with the orthorhombic symmetry of the unit cell. From an hexagonal AO_3 layer with a_{2H} and b_{2H} parameters, the

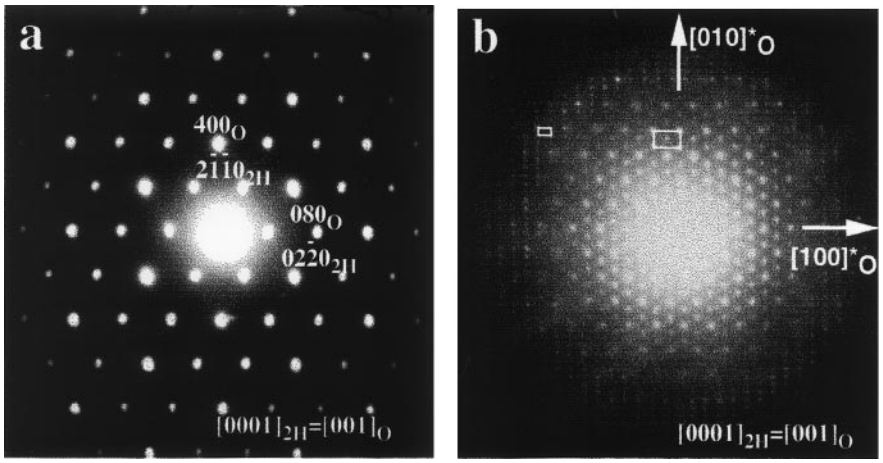

FIG. 3. (a) SAED pattern of o-$Ba_8Co_7O_{21}$ along $[0001]_{2H}$; (b) microdiffraction pattern along the same projection.

substitution of three oxygen atoms by one *B* cation following the $[11\bar{2}0]_{2H}$ and equivalent directions leads to a layer with the A_3BO_6 composition and rhombohedral symmetry ($a_R = b_R = \sqrt{3}a_{2H}$), as shown by Subramanian and Darriet (4). However, if such substitution takes place along $[10\bar{1}0]_{2H}$ and equivalent directions, the resulting layer, with the composition $A_8B_2O_{18}$, shows orthorhombic symmetry and parameters $a_o = 2a_{2H}$, $b_o = 2\sqrt{3}a_{2H}$ (15). The features of this layer are compatible with the above diffraction data. Figure 4 shows a schematic representation of an $A_8B_2O_{18}$ layer in comparison to the stoichiometric AO_3 layer (or A_8O_{24} per orthorhombic unit) and the rhombohedral layer (A_3BO_6).

Besides, the four-fold superlattice along the *c* axis suggests this phase is composed of eight layers. Taking into account the chemical composition of the sample, $Ba_8Co_7O_{21}$ ($z = 8$), this material must be formed by four A_8O_{24} layers and four $A_8B_2O_{18}$ layers hexagonally stacked. In order to determine the sequence of these layers a HREM study has been performed.

Figure 5a shows the HREM image corresponding to the $[100]_o//[\bar{2}110]_{2H}$ zone axis. The contrast alternation observed in the thinnest area of this crystal (zone A) shows that the hexagonal packing is maintained. In the thickest area (zone B) besides the basic 2H substructure, an additional ordering doubling b_{2H} and c_{2H} is observed. Along the c_{2H} axis, the contrast variation corresponds with the alternation of a bright dot with three less intense dots. These bright dots could be associated with individual columns of metallic atoms. The different brightness of the dots corres-

TABLE 1
Observed and Calculated Powder XRD Data for $Ba_8Co_7O_{21}$ ($a = 1.148(3)$ nm, $b = 1.989(4)$ nm, $c = 1.746(6)$ nm; $Z = 8$)

d_{obs} (nm)	d_{calc} (nm)	I/I_0	*hkl*
0.8650	0.86425	0.4	111
0.4972	0.49737	0.4	040
0.3281	0.32814	98	044
0.2866	0.28708	100	400
0.2488	0.24867	6.3	080
0.2184	0.21833	6.2	008
0.2159	0.21609	48.2	084
0.1998	0.19991	3.9	048
0.1848	0.18386	1.8	139
0.1737	0.17378	18	408
0.1723	0.17220	14	11$\underline{10}$
0.16582	0.16579	1.6	0$\underline{12}$0
0.1638	0.16407	2.5	088

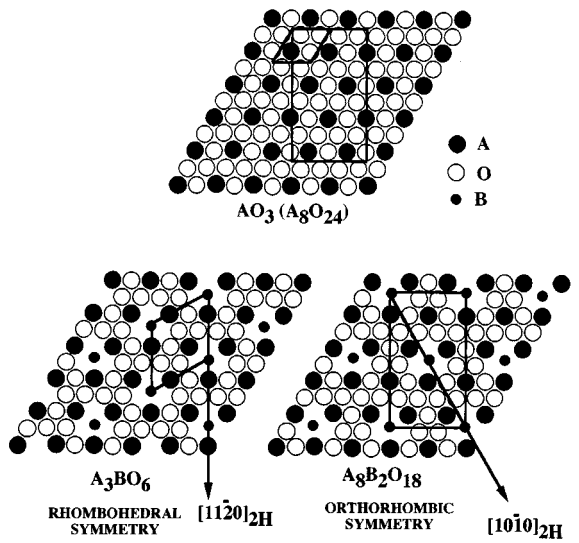

FIG. 4. Schematic representations of AO_3 (or A_8O_{24} per orthorhombic unit), rhombohedral A_3BO_6, and orthorhombic $A_8B_2O_{18}$ layers.

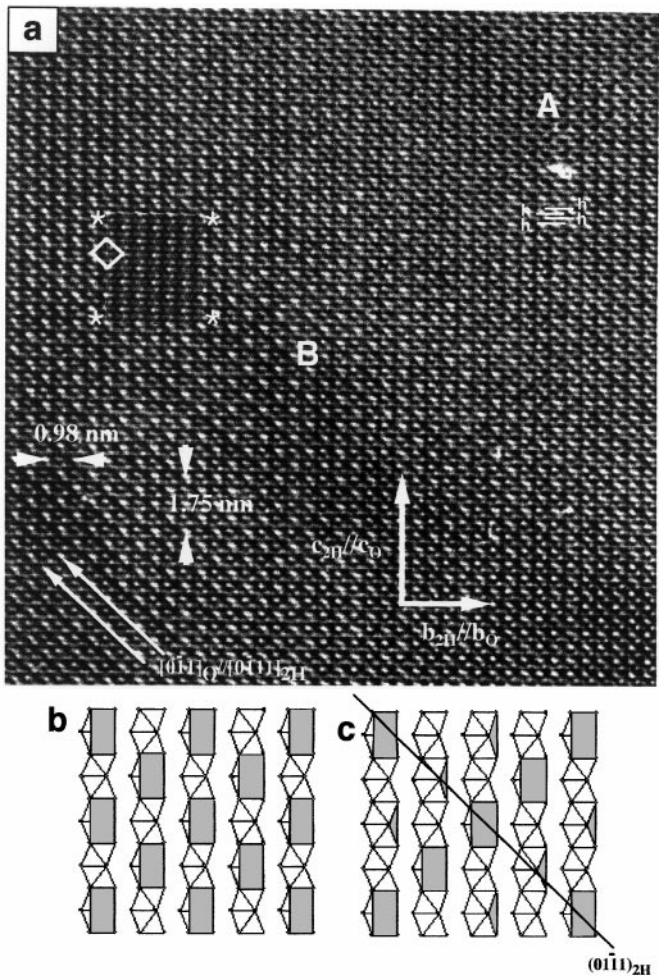

FIG. 5. (a) HREM image of o-$Ba_8Co_7O_{21}$ along $[100]_o$. A simulated image is shown in the inset ($\Delta t = 5$ nm, $\Delta f = 0$ nm). Schematic representation of the structural models **A** (b) and **B** (c) projected along $[100]_o$. Both models are formed by parallel isolated rows of polyhedra, running parallel to the *c*-axis; the difference between them resides in the polyhedral distribution of the chains.

ponds to sites with different electronic density, in such a way that the brightest dots can be assimilated to the Ba configuration in between the Co columns, and the three less intense dots should correspond only to the Ba configuration. The same situation can be found along the b_o axis if a displacement of $\frac{1}{4}c_o$ is considered. As a consequence, rows of low-intensity equivalent dots alternate, parallel to the b_o axis, with rows of nonequivalent dots. This contrast variation can be attributed to A_8O_{24} layers alternating with $A_8B_2O_{18}$ layers in a 1:1 sequence. This layer sequence could give rise to two different structural models (**A** and **B**).

Figure 5b represents the first model (model **A**) viewed along the $[100]_o$ ($//[\bar{2}110]_{2H}$) direction. Along this direction (perpendicular to the image plane), the structure can be described as formed by isolated rows of octahedra sharing faces, running parallel to the *c*-axis, alternating with similar isolated rows, now composed of two octahedra and one trigonal prism sharing faces. Besides, the last row is displaced $\frac{1}{4}c_o$ following the b_o direction.

The second one (model **B**), as represented in Fig. 5c along the same projection, can be described as formed by isolated rows, running parallel to the *c*-axis, of six octahedra and one trigonal prism. Along the b_o axis, one row is displaced $\frac{1}{4}c_o$ with respect to the adjacent one, and along the a_o direction, rows are displaced $\frac{1}{2}c_o$. Both models could fit with the features observed in the image. In both cases, the disposition of Co prisms is in agreement to the rectangular array of the bright dots observed in the image of Fig. 5a (marked in the image). Besides, light and dark bands parallel to $[0\bar{1}11]_{2H}//[0\bar{1}1]_o$ (marked with arrows) correspond to parallel bands of high electronic density (Co prisms) and relatively low density (Co octahedra).

However, the structural model **B** is the most probable since the first one leads to only a two-fold superstructure along c_{2H} axis. Moreover, the following projection allows us to confirm the second structural model as the most probable.

The spatial arrangement of the polyhedra rows along the b_{2H} axis ($[\bar{1}10]_o$) can be seen in the HREM image shown in Fig. 6a. The thinnest area (zone A) of the crystal shows only the hexagonal sequence of the 2H sublattice. In the thickest area (zone B) only equivalent layers are solved, i.e., ($\ldots AAA \ldots$) or ($\ldots BBB \ldots$); however, a difference in the intensities of the bright dots can be appreciated. As can be observed, two bright dots alternate with two less intense dots along the c_o (c_{2H}) and a_{2H} ($[110]_o$) axes. This contrast variation is not compatible with the first structure model (**A**) depicted in this projection in Fig. 6b. This polyhedra arrangement should lead to one row, parallel to the *c*-axis, of equivalent bright dots alternating to another row of less intense dots along the $[110]_o$. However, it agrees with the features of the second structural model (**B**) (projected along the $[\bar{1}10]_o$ direction in Fig. 6c). As can be seen, perpendicular to the image plane, Co prisms and Co octahedra are superimposed at $z = 0, \frac{1}{4}$. This situation leads to two positions with equivalent electronic density associated with the brightest dots in the experimental micrograph. In the positions corresponding to $z = \frac{1}{2}$ and $\frac{3}{4}$, only octahedral sites are placed and the contrast is modified with respect to the previous ones. Along the a_{2H} axis ($[110]_o$), the same situation can be found if a displacement of $\frac{1}{2}c_o$ is considered as corresponding to the relative disposition of prisms and octahedra along this axis. Once again, it is worth emphasizing that light and dark bands parallel to $[\bar{1}\bar{1}1]_o//[\bar{1}012]_{2H}$ are superimposed (marked with arrows) which correspond to parallel bands of high electron density (Co prisms) and relatively low density (Co octahedra).

HREM images have been simulated by using the Mac Tempas package from the atomic coordinates (Table 2) resulting from the structural model depicted in Fig. 7.

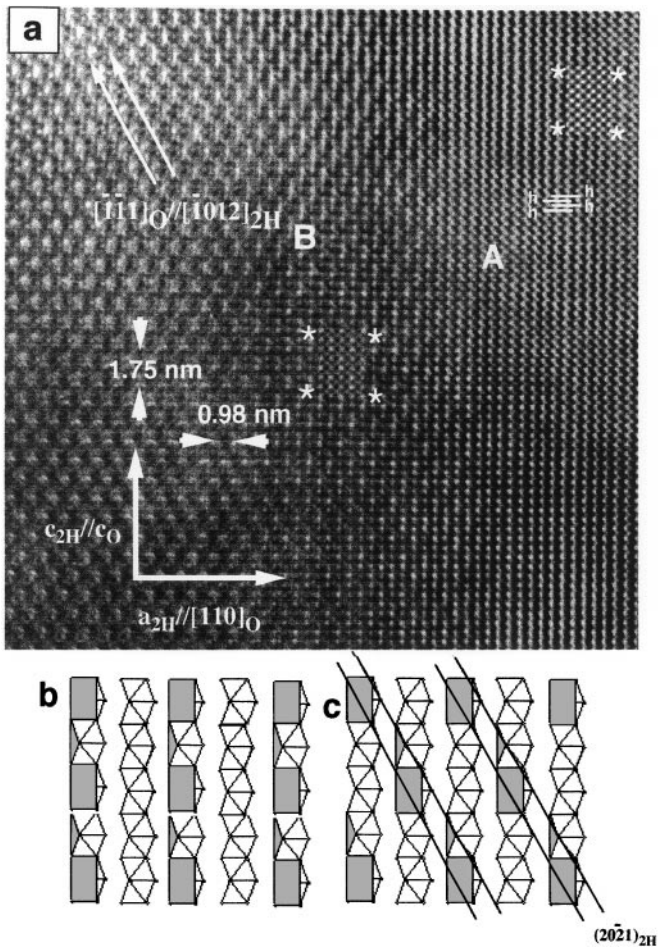

FIG. 6. (a) HREM image of o-$Ba_8Co_7O_{21}$ along $[\bar{1}10]_o$. Simulated images corresponding to zone A ($\Delta t = 2.5$ nm, $\Delta f = -45$ nm) and zone B ($\Delta t = 5$ nm, $\Delta f = -20$ nm) are shown. (b) Schematic representation along $[\bar{1}10]_o$ of the structural model **A**. (c) Schematic representation along $[\bar{1}10]_o$ of the structural model **B**.

TABLE 2
Atomic Coordinates for $Ba_8Co_7O_{21}$ (SG *Fd2d*)

Atom	site	*x*	*y*	*z*
Ba1	8a	0	0.1875	0
Ba2	8a	0	0.6875	0
Ba3	16b	0.25	0.4375	0
Ba4	16b	0.25	0.0625	0.125
Ba5	16b	0.75	0.0625	0.125
Co1[a]	8a	0	0	0
Co2	16b	0	0	0.1875
Co3	16b	0	0	0.3125
Co4	16b	0	0	0.4375
O1	16b	0	0.0625	0.125
O2	8a	0	0.4375	0
O3	16b	0	0.4375	0.25
O4	16b	0	0.5625	0.125
O5	16b	0.375	0.0625	0
O6	16b	0.125	0.3125	0
O7	16b	0.375	0.3125	0
O8	16b	0.125	0.1875	0.125
O9	16b	0.375	0.1875	0.125
O10	16b	0.125	0.4375	0.125
O11	16b	0.625	0.4375	0.125

[a] Cobalt atom in prismatic coordination.

Simulated images are included in the insets of Figs. 5a and 6a. A good fit is obtained for both projections.

The ideal crystal structure of the o-$Ba_8Co_7O_{21}$ phase can be described as formed by isolated rows of polyhedra parallel to the *c*-axis. Each row is formed by six octahedra and one trigonal prism sharing faces. In the rows of polyhedra parallel to either the *a*- or *b*-axes the trigonal prisms are displaced along the *c*-axis. Following the a_{2H} axis, the prisms of a given row are displaced $2c_{2H}$ ($\frac{1}{2}c_o$) with respect to the adjacent one. Following the b_{2H} axis, each prism is displaced c_{2H} ($\frac{1}{4}c_o$) with respect to the next row. As a consequence, the basic 2H hexagonal subcell is doubled in both the a_{2H} and b_{2H} axes, leading to the proposed orthorhombic unit cell which includes eight-unit formula $Ba_8Co_7O_{21}$. This structural model can be derived from the ordered sequence of one $A_8B_2O_{18}$ and one A_8O_{24} layer along the *c*-axis. Between two succesive A_8O_{24} and $A_8B_2O_{18}$ layers, six octahedral sites and one prismatic site are generated per unit cell, as schematically represented in Fig. 8. If we suppose that this situation corresponds to Co trigonal prisms marked with ① in Fig. 7, Co atoms marked with ②, ③, and ④ can be generated in the same way, if we consider a displacement from the origin of the previous layers at ($\frac{1}{4}\frac{1}{4}$), ($\frac{1}{2}$ 0) and ($\frac{1}{4}\frac{3}{4}$), respectively.

As we have previously mentioned, this orthorhombic phase constitutes the first example of polymorphism re-

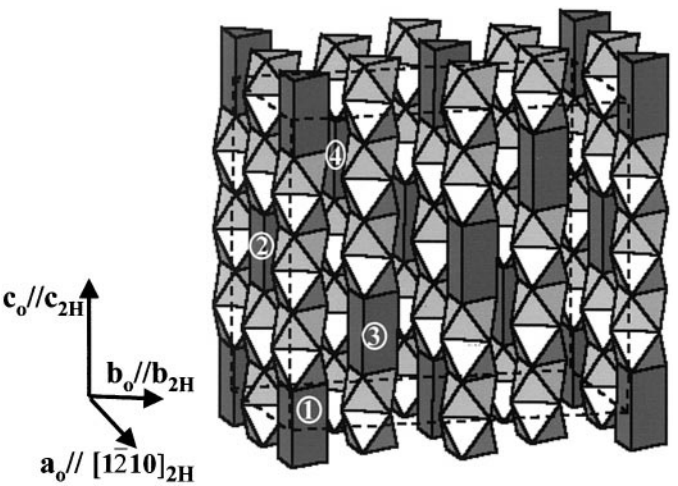

FIG. 7. Structural model proposed for o-$Ba_8Co_7O_{21}$.

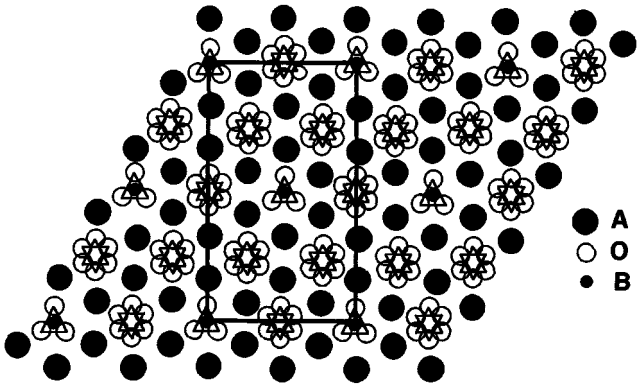

FIG. 8. Schematic representation of the octahedral and prismatic sites generated by two successive A_8O_{24} and $A_8B_2O_{18}$ layers hexagonally stacked.

ported in the 2H-related monodimensional oxides. The two phases, orthorhombic and trigonal, can be derived from a hcp sequence of mixed layers, but neither the type nor the disposition of layers constituting the structural framework is the same. As previously reported (11), the hexagonal stacking of mixed Ba_3CoO_6 and Ba_3O_9 layers in a $(Ba_3CoO_6/2Ba_3O_9/Ba_3CoO_6/1Ba_3O_9)$ sequence forms the structure of the trigonal $Ba_8Co_7O_{21}$ composed of isolated polyhedra rows, running parallel to the *c*-axis, formed by one trigonal prism and six octahedra sharing faces.

The same polyhedra sequence is maintained in the rows that constitute the orthorhombic phase, but this polyhedra succession is now generated from a different sequence of different type of layers. Effectively, as we have shown, the alternation of one A_8O_{24} layer and one $A_8B_2O_{18}$ layer also leads to rows of one trigonal prism and six octahedra, but the spatial arrangement between the chains is clearly different from that found in the trigonal phase as can be easily observed along the $[1\bar{1}00]_{2H}$ projection (see Fig. 7). In the trigonal phase, the Co atoms in prismatic coordination are superimposed along the direction perpendicular to the image plane (see Fig. 9a). However, in the equivalent projection of the orthorhombic phase, octahedra and prisms alternate along the same perpendicular direction (see Fig. 10a) The corresponding HREM images clearly revealed these different structural characteristics. Figure 9b shows the structure image along $[1\bar{2}10]_t$ ($//[1\bar{1}00]_{2H}$) of trigonal $Ba_8Co_7O_{21}$. Following the *c*-axis, the observed alternation of two bright dots with six less bright dots has been interpreted as due to the alternation of one Co prism and six Co octahedra along this direction. This situation leads to light and dark bands parallel to $[\bar{1}011]_t$, as marked with an arrow in the image. This direction corresponds to that in which Co atoms in prism coordination are aligned. These atoms are contained in the $(88i6)_{2H}$ planes, which correspond to the modulation reciprocal direction (see SAED pattern of Fig. 9c), being the wave vector $\mathbf{k} = \frac{1}{3}(a^*_{2H} + b^*_{2H}) + \frac{1}{8}c^*_{2H}$. Figure 10a shows the structure image corresponding to the orthorhombic phase, along the same projection. Now, along the [001] direction, four bright dots alternate with four less bright. In this projection, as can be seen in Fig. 10b, the superposition of Co prisms and Co octahedra leads to two positions with equivalent electronic density ($z = 0, \frac{1}{8}, \frac{1}{4}, \frac{3}{8}$). The positions at $z = \frac{1}{2}, \frac{5}{8}, \frac{3}{4}$, and $\frac{7}{8}$ correspond only to Co octahedra which appear in the image as the less bright positions. The rows of brightest dots also correspond to the direction in which Co prisms are aligned. It is worth mentioning that a modulation is also observed in this phase along $[44\bar{8}2]^*_{2H}$ (see Fig. 2d), being the modulation vector $\mathbf{k} = \frac{1}{2}(a^*_{2H} + b^*_{2H}) + \frac{1}{8}c^*_{2H}$. This direction is perpendicular to the planes containing Co atoms in prismatic sites, suggesting that the modulation origin is, as proposed for the rhombohedral or trigonal phases, due to the displacement of Co atoms in these sites in such a way that they are in off-centered positions along the trigonal axis (11, 16). Image calculations fit with the experimental one in both cases, as can be seen in the insets of Figs. 9b and 10a.

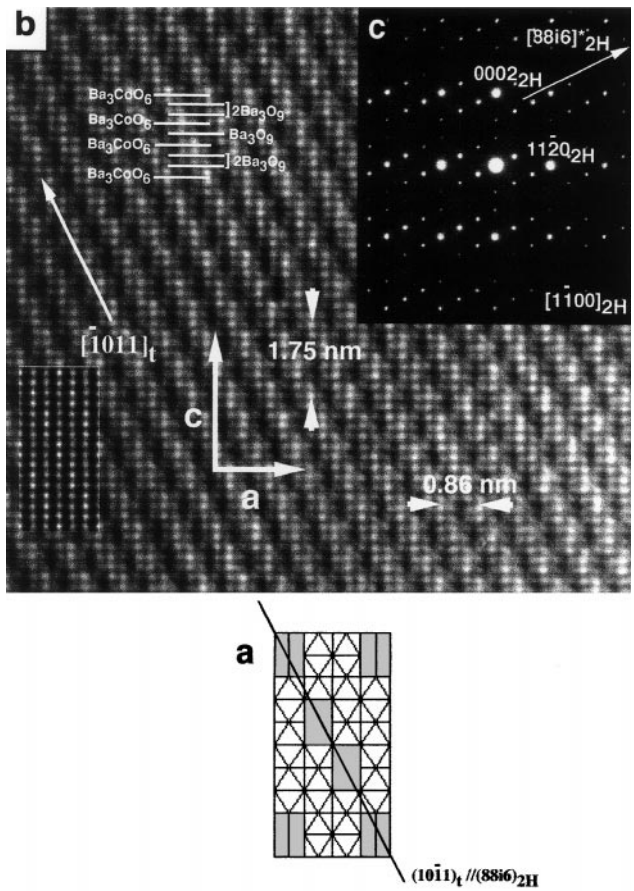

FIG. 9. (a) Schematic representation along $[\bar{1}100]_{2H}$ corresponding to t-$Ba_8Co_7O_{21}$(12). (b) Corresponding HREM image. A simulated image is shown in the inset ($\Delta t = 7$ nm, $\Delta f = -95$nm). (c) Corresponding SAED pattern.

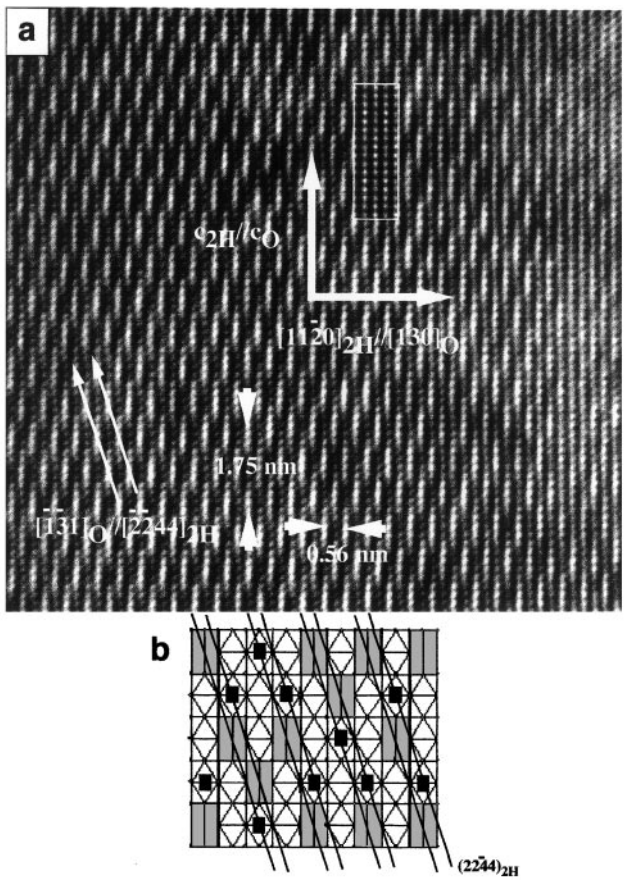

FIG. 10. (a) HREM image along along $[\bar{1}100]_{2H}$ corresponding to o-$Ba_8Co_7O_{21}$. A calculated image ($\Delta t = 4$ nm, $\Delta f = -95$ nm) is shown in the inset. (b) Schematic representation along $[\bar{1}100]_{2H}$ corresponding to o-$Ba_8Co_7O_{21}$. ■ refers to Co prims along b_o.

On the basis of these results, it can be deduced that a given octahedra–prism sequence along an isolated row can be attained always from a hexagonal stacking which can be formed by different type of layers. This seems to indicate that any rhombohedral or trigonal phase of the homologous series $(A_3B_2O_6)_\alpha(A_3B_3O_9)_\beta$ could have the corresponding orthorhombic polymorph. Obviously, the limit in the orthorhombic phases is defined by a sequence of layers $A_8B_2O_{18}$; therefore, the lowest composition would be $A_{16}B_{12}O_{36}$ ($A_4B_3O_9$). This suggests that polymorphism can be a general rule better than an exception in the Ba–Co–O system. In order to prove this statement, new situations will be explored in the near future.

ACKNOWLEDGMENTS

We acknowledge the financial support of CICYT (Spain) through Research Project MAT98-0648.

REFERENCES

1. J. J. Lander, *Acta Crystallogr.* **4,** 148 (1951).
2. J. J. Randall and L. Katz, *Acta Crystallogr.* **12,** 519 (1959).
3. K. Boulahya, M. Parras and J. M. González-Calbet, *Chem. Mater.* **12**(1), 25 (2000).
4. J. Darriet and M. A. Subramanian, *J. Mater. Chem.* **5,** 543 (1995).
5. P. D. Battle, G. R. Blake, J. Darriet, J. G. Gore, and F. Weill, *J. Mater. Chem.* **7** (8), 1559 (1997).
6. P. D. Battle, J. C. Burley, E. J. Cussen, J. Darriet, and F. Weill, *J. Mater. Chem.* **9,** 479 (1999).
7. W. T. A. Harrison, S. L. Hegwood, and A. J. Jacobson, *J. Chem. Soc., Chem. Commun.* 1953 (1995).
8. H. Fjellvag, E. Gulbrandsen, S. Aasland, A. Olsen, and B. C. Hauback, *J. Solid State Chem.* **124,** 190 (1996).
9. J. A. Campá, E. Gutiérrez-Puebla, M. A. Monge, I. Rasines, C. Ruiz-Valero, *J. Solid State Chem.* **108,** 230 (1994).
10. M. Huvé, C. Renard, F. Abraham, G. Van Tendeloo, and S. Amelinckx, *J. Solid State Chem.* **135,** 1 (1998).
11. K. Boulahya, M. Parras, and J. M. González-Calbet, *J. Solid State Chem.* **142,** 419 (1999).
12. K. Boulahya, M. Parras, and J. M. González-Calbet, *J. Solid State Chem.* **145,** 116 (1999).
13. H. Taguchi, Y. Takeda, F. Kanamara, M. Shimada, and M. Kaizomi, *Acta Crystallogr. B* **33,** 1299 (1977).
14. J. P. Morniroli and J. W. Steeds, *Ultramicroscopy* **45,** 219 (1992).
15. J. M. González-Calbet, K. Boulahya, and M. Parras, Proc. 14th Int. Congress on Electron Microscopy, Bristol. 1998, Vol. III, p. 331.
16. M. Evain, F. Boucher, O. Gourdon, V. Petricek, M. Dusek, and P. Berdicka, *Chem. Mater.* **10,** 3068 (1998).